Author(s): Constantinides, Christos P.; Lawson, Daniel B.; Zissimou, Georgia A.; Berezin, Andrey A.; Mailman, Aaron; Manoli, Maria; Kourtellaris, Andreas; Leitus, Gregory M.; Clérac, Rodolphe; Tuononen, Heikki M.; Koutentis, Panayiotis A.

Title: Polymorphism in a π stacked Blatter radical : structures and magnetic properties of 3-(phenyl)-1-(pyrid-2-yl)-1,4-dihydrobenzo[e][1,2,4]triazin-4-yl

Year: 2020

Version: Accepted version (Final draft)

Polymorphism in a π Stacked Blatter Radical: Structures and Magnetic Properties of 3-(Phenyl)-1-(pyrid-2-yl)-1,4-dihydrobenzo[e][1,2,4]triazin-4-yl

Christos P. Constantinides,*[a] Daniel B. Lawson,[a] Georgia A. Zissimou,[b] Andrey A. Berezin,[b] Aaron Mailman,[c] Maria Manoli,[b] Andreas Kourtellaris,[b] Gregory M. Leitus,[d] Rodolphe Clérac,[e] Heikki M. Tuononen,[c] and Panayiotis A. Koutentis[b]

[a] Department of Natural Sciences, University of Michigan-Dearborn, 4914 Evergreen Road, Dearborn, MI 48128-1491, United States. E-mail: cconst@umich.edu Fax: +01 3135934937 Tel: +01 3135836728

[b] Department of Chemistry, University of Cyprus, P.O. Box 20537, 1678 Nicosia, Cyprus

[c] Department of Chemistry, NanoScience Center, University of Jyväskylä, P. O. Box 35, FI-40014 Jyväskylä, Finland

[d] Chemical Research Support Unit, Weizmann Institute of Science, 7610001 Rehovot, Israel

[e] Univ. Bordeaux, CNRS, Centre de Recherche Paul Pascal, UMR 5031, 33600 Pessac, France

Abstract

3-(Phenyl)-1-(pyrid-2-yl)-1,4-dihydrobenzo[e][1,2,4]triazin-4-yl (**2**) demonstrates the first example of polymorphism in the family of Blatter radicals. Two polymorphs, **2α** and **2β**, have been identified and characterized by single crystal X-ray diffractometry and magnetic susceptibility measurements to investigate their magnetism-structure correlations. Both

polymorphs form one-dimensional (1D) π stacks of evenly spaced radicals with distinctly different π-π overlap modes. Within the 1D π stacks, radicals are located at evenly interplanar distances, 3.461 Å for 2α and 3.430 Å for 2β. Magnetic susceptibility studies indicate that both polymorphs exhibit antiferromagnetic interactions inside their 1D π stacks. The magnetic susceptibility data are best interpreted in terms of a regular chain model of antiferromagnetically coupled quantum spins ($H = -2J \sum_i \vec{S_i} \bullet \overrightarrow{S_{i+1}}$) with exchange-interactions of $J/k_B = -36.7(3)$ K ($-25.5(2)$ cm^{-1}) for 2α and $J/k_B = -72(3)$ K ($-50(2)$ cm^{-1}) for 2β. For polymorph 2β, a crossover on the magnetic susceptibility around 20 K suggests the presence of a phase transition, which might be related to dimerization of the radicals along the chain. DFT calculations support the experimental structure-magnetism results and the antiferromagnetic nature of the local interactions between radicals within the 1D π stacks.

1. Introduction

1,3-Diphenyl-1,4-dihydrobenzo[*e*][1,2,4]triazin-4-yl (**1**) *aka* Blatter radical (Fig. 1) was first prepared in 1968[1] and did not receive much attention[2-6] until 1996 when F. Wudl showed that it forms a pressure sensitive semiconductor with tetracyanoquinodimethane (TCNQ).[7] Blatter radical **1** is stable to oxygen and moisture,[8] and can readily be sublimed without degradation.[9,10] Owing to these exceptional physical properties, we have systematically developed new synthetic procedures[11-17] to broaden access and significantly expand the structural diversity of Blatter radicals.[18-20] These efforts have led to Blatter-type radicals with new physical properties and applications.[10,21-34] Various one-dimensional (1D) magnetic properties[21-24,28,30-34] and two systems with a first order structural phase transition inducing magnetic bistability[25,29] have been reported. Blatter radicals have also been used in chemical synthesis. For example, they can act as initiators

in controlled polymerizations,[35-38] as organic paramagnetic ligands in metal coordination complexes,[39-41] and as building blocks in high-spin diradicals and biradicaloids.[32,42,43] Blatter-type radicals can form stable thin films (without degradation) while retaining their paramagnetic character.[44,45] Efforts to understand the Blatter radical/inorganic 'spinterfaces' are underway,[46,47] which coud open the possibility to use these radicals in spintronic devices.[48] Other Blatter-type radical applications that have emerged during the past five years include: (i) photodetectors;[49,50] (ii) emissive materials for OLEDs;[51] (iii) pH sensors;[30] (iv) liquid crystalline photoconductors,[52-55] and, more recently, (v) as electroactive building blocks in polymers of purely organic batteries.[56] These exciting applications rely on the discovery of "structure-property" relationships that enable a better understanding of the intrinsic microscopic and macroscopic properties of these radicals. Herein, as part of our ongoing investigations in magnetism-structure correlations of Blatter-type radicals, we report the solid state characterizations of 3-(phenyl)-1-(pyrid-2-yl)-1,4-dihydrobenzo[*e*][1,2,4]triazin-4-yl (**2**) (Fig. 1), a Blatter-type radical that demonstrates polymorphism.

Polymorphism in organic radicals is a common phenomenon.[57] It occurs as a result of different crystal packings with typically small differences in their lattice energy.[58] Polymorphism is well documented for thiazyl radicals.[59-67] However, for hydrazyls only one example of a verdazyl radical was recently reported.[68] The 1,5-diisopropyl-3-(4'-carboxyphenyl)-6-oxoverdazyl crystallizes as two polymorphs with markedly different crystal packings and magnetic properties.[68] Polymorphism in Blatter-type radicals could potentially be more prevalent owing to the extended spin delocalization and the large SOMO surface of the benzotriazinyl core. This characteristic leads to many potential sites for intermolecular interactions in the crystal packing and thus opportunities for polymorphism. In the present work, 3-(phenyl)-1-(pyrid-2-yl)-1,4-

dihydrobenzo[e][1,2,4]triazin-4-yl (**2**) (Fig. 1) is shown to crystallize in two polymorphs, **2α** and **2β**, consisting of supramolecular chains of equidistant radicals exhibit antiferromagnetic exchange interactions despite the distinctly different crystal packing.
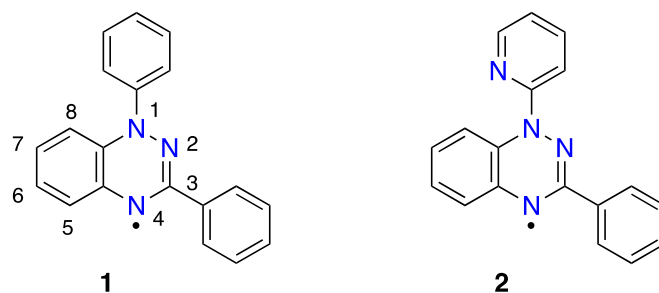

Fig. 1 Molecular structures of benzotriazinyls **1** and **2** showing atom numbering.

2. Experimental

2.1 Synthesis

As we have previously reported,[13] the synthesis of the 3-(phenyl)-1-(pyrid-2-yl)-1,4-dihydrobenzo[e][1,2,4]-triazin-4-yl radical **2** involves the preparation of N'-(2-nitrophenyl)-N'-(pyrid-2-yl)benzohydrazide (**3**) which upon an acid-catalysed, tin-mediated reductive cyclodehydration and subsequent air oxidation affords **2** (Scheme 1).
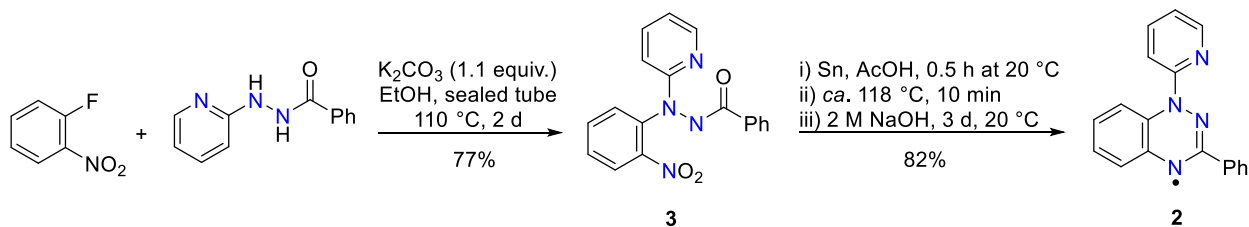
Scheme 1 Synthetic route to radical **2**.

2.2 EPR and Cyclic Voltammetry

The solid-state and solution EPR spectra (CH_2Cl_2, *ca.* 20 °C) of radical **2** have been previously reported, and we summarize the data here.[13] The solution EPR spectrum of radical **2** is typical of benzotriazinyls with the largest ^{14}N hyperfine coupling constant (hfcc) located at N1 followed by N4 and N2 ($a_{N1} \gg a_{N4} > a_{N2}$).[4] The experimentally determined hyperfine coupling constants for radical **2** are a_{N1} (6.74 G), a_{N2} (4.88 G), a_{N4} (4.9. G) with $g_{solution} = 2.0040$ and $g_{solid} = 2.0046$ which compare well with the values deduced from the modelling of the magnetic susceptibility data (*vide infra*). Cyclic voltammetry (CV) measurements of radical **2** (1mM in CH_2Cl_2 containing *n*-Bu_4NBF_4 (0.1 M) as electrolyte, Ag/AgCl as reference electrode, 50 mV s^{-1} scan rate, *ca.* 20 °C, Fc/Fc$^+$as internal reference), show two fully reversible oxidation $E_{1/2}$ (*ox*) = 0.24 V and reduction waves $E_{1/2}$ (red) = –0.82 V and E_{cell} = 1.06 V.

2.3 Single crystal and powder X-ray diffractometry

Single crystal X-ray diffraction data were collected on an Agilent SuperNova diffractometer, equipped with an Atlas detector and Cu-Kα radiation source ($\lambda = 1.5418$ Å). Suitable crystals were attached to MiTeGen micro-mounts with Fromblin® Y oil and transferred to a goniostat where they were cooled for data collection. Unit cell dimensions were determined and refined by using 2674 reflections ($4.75 \leq \theta \leq 74.49°$) for polymorph **2α** and 2797 ($4.50 \leq \theta \leq 76.65°$) for polymorph **2β**. Data acquisitions, reductions and empirical absorption corrections were applied using CrysAlis PRO software.[69] The structures were solved by direct method and refined on F^2 using full-matrix least squares using SHELXL.[70-71] The non-H atoms were treated anisotropically. The hydrogen atoms were placed in calculated, ideal positions and refined as riding on their respective carbon atoms. Crystallography figures were generate using Mercury.[72] Powder X-ray diffraction (PXRD)

patterns for samples **2α** and **2β** were recorded on a Shimazdu 6000 Series X-ray diffractometer at room temperature (Cu Kα radiation, $\lambda = 1.5418$ Å).

Crystal refinement data of 3-(phenyl)-1-(pyrid-2-yl)-1,4-dihydrobenzo[e][1,2,4]triazin-4-yl (**2α**) (CCDC 1955680): $C_{18}H_{13}N_4$, $MW = 285.32$ g mol^{-1}, Orthorhombic space group $P2_12_12_1$, $a = 7.1656(3)$, $b = 10.9705(4)$, $c = 17.5843(6)$ Å, $V = 1382.31(9)$ Å^3, $Z = 4$, $T = 120.01(10)$ K, $\rho_{calcd} = 1.371$ g cm^{-3} $2\theta_{max} = 77.49$. Refinement of 199 parameters on 2674 independent reflections out of 5012 measured reflections ($R_{int} = 0.0281$) led to $R_1 = 0.0388$ [$I > 2\sigma(I)$], $wR_2 = 0.1001$ (all data), and $S = 1.040$ with the largest difference peak and hole of 0.163 and –0.177 e^{-3}, respectively.

Crystal refinement data of 3-(phenyl)-1-(pyrid-2-yl)-1,4-dihydrobenzo[e][1,2,4]triazin-4-yl (**2β**) (CCDC 1955684): $C_{18}H_{13}N_4$, $MW = 285.32$ g mol^{-1}, Monoclinic space group $P\ 2_1/c$, $a = 19.7893(9)$, $b = 3.76820(10)$, $c = 19.7322(8)$ Å, $V = 1337.94(10)$ Å^3, $Z = 4$, $T = 120.00(10)$ K, $\rho_{calcd} = 1.416$ g cm^{-3}, $2\theta_{max} = 76.65$. Refinement of 199 parameters on 2797 independent reflections out of 9981 measured reflections ($R_{int} = 0.0267$) led to $R_1 = 0.0418$ [$I > 2\sigma(I)$], $wR_2 = 0.1196$ (all data), and $S = 1.030$ with the largest difference peak and hole of 0.222 and –0.266 e^{-3}, respectively.

2.4 Magnetic Susceptibility Measurements

Magnetic measurements were performed on a Quantum Design SQUID magnetometers MPMS-XL (Quantum Design, San Diego, CA, USA) and MPMS3-VSM at temperatures between 1.8 and 300 K, and dc magnetic fields ranging from –7 to +7 T. The measurements were carried out on polycrystalline samples (22.21, 21.13 and 21.6 mg for **2α**, and 21.35, 15.6, 14.5 and 15.1 mg for **2β**) introduced in a sealed polyethylene bag (3×0.5×0.02 cm; typically, 18-22 mg) or gelatin

capsules. Prior to the main experiments, the field-dependent magnetization was measured at 100 K on each sample to detect the possible presence of any bulk ferromagnetic impurities. Paramagnetic materials should exhibit a perfect linear dependence of magnetization that extrapolates to zero at zero dc field and all samples appeared to be free of any bulk ferromagnetic impurities. The magnetic data were corrected for the sample holder and intrinsic diamagnetic contributions.[73]

2.5 Computational Methodology

Exchange coupling constants were calculated using broken symmetry density functional theory (BS-DFT) by mapping the energies of the calculated states to the diagonal elements of the Heisenberg-Dirac-van Vleck Hamiltonian $H = -2J_{comp} \widehat{S_1} \cdot \widehat{S_2}$, where J_{comp} is the calculated exchange-coupling constant and $\widehat{S_1}$ and $\widehat{S_2}$ are spin operators acting on two spin sites.[74] The energies of the broken symmetry singlet and triplet states were determined by single point calculations using geometries extracted from crystal structures. Seven different functionals, namely B3LYP, X3LYP, CAM-B3LYP, ωB97x, LC-ωHPBE, M06-2X and M15, were employed together with the large def2-TZVPP basis sets.[75] B3LYP is the classic three-parameter hybrid functional consisting of Becke's 88 exchange functional[76] and the correlation functional of Lee, Yang and Parr,[77] whereas X3LYP replaces Becke's 88 exchange with an improved functional developed to provide a better description of non-bonded interactions, spin states and thermochemical properties.[78] CAM-B3LYP is a hybrid functional which combines B3LYP with a long-range correction based on the Coulomb-attenuating method.[79] ωB97X[80] is a long-range corrected functional based on Becke's work, whereas LC-ωHPBE[81] is Henderson's version of the long-range-corrected LC-ωPBE functional of Vydrov.[82-84] M06-2X[85,86] is a global hybrid with

54% HF exchange and empirically parameterized only for non-metals. MN15[87,88] is a newer version of M06 with 44% HF exchange and parameterized for multi-reference systems and noncovalent interactions. All calculations were performed with Gaussian16[89] using XSEDE[90] resources and services.

3. Results and Discussion

3.1 Crystal Structures

Radical **2** crystalizes in two polymorphs **2α** (CCDC 1955680) and **2β** (CCDC 1955684). Single crystals suitable for X-ray diffraction studies were obtained by slow cooling of a dilute and concentrated *n*-hexane solution for **2α** and **2β**, respectively. Careful recrystallization is required to avoid crystallization of both polymorphs as mixtures. Polymorph **2β** comes out rapidly from a hot super saturated solution as it cools down to room temperature and is, tentatively, the kinetic polymorph or a metastable kinetic polymorph. Polymorph **2α** comes out of solution slowly once at room temperature and is, tentatively, the thermodynamic polymorph. Both crystal structures were collected at 100(2) K. Polymorph **2α** crystallizes in the orthorhombic space group $P\ 2_12_12_1$ and polymorph **2β** in the monoclinic space group $P\ 2_1/c$. Both polymorphs contain one molecule in the asymmetric unit. The intramolecular bond angles and bond lengths are similar to that of other benzotriazinyls,[21-27] however, there is a significant difference in the geometry of the amidrazonyl moiety. In polymorph **2α**, the 1,2,4-amidrazonyl moiety adopts a shallow boat conformation with deviations of the N1 and N3 atoms from the mean plane of C2, C3, N2, C1 of 0.09 and 0.06 Å, respectively (Fig. 2, top). A similar amidrazonyl structure was observed in 1,3-diphenyl-7-trifluoromethyl-1,4-dihydrobenzo[*e*][1,2,4]triazin-4-yl.[10]
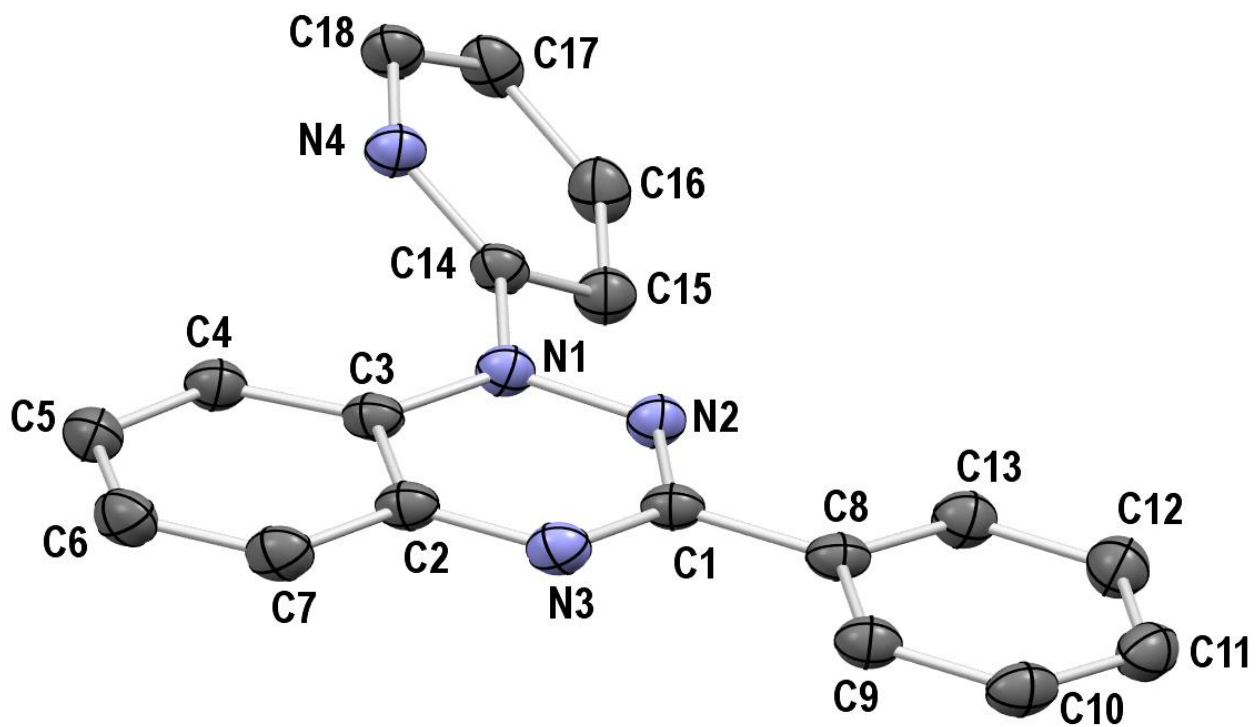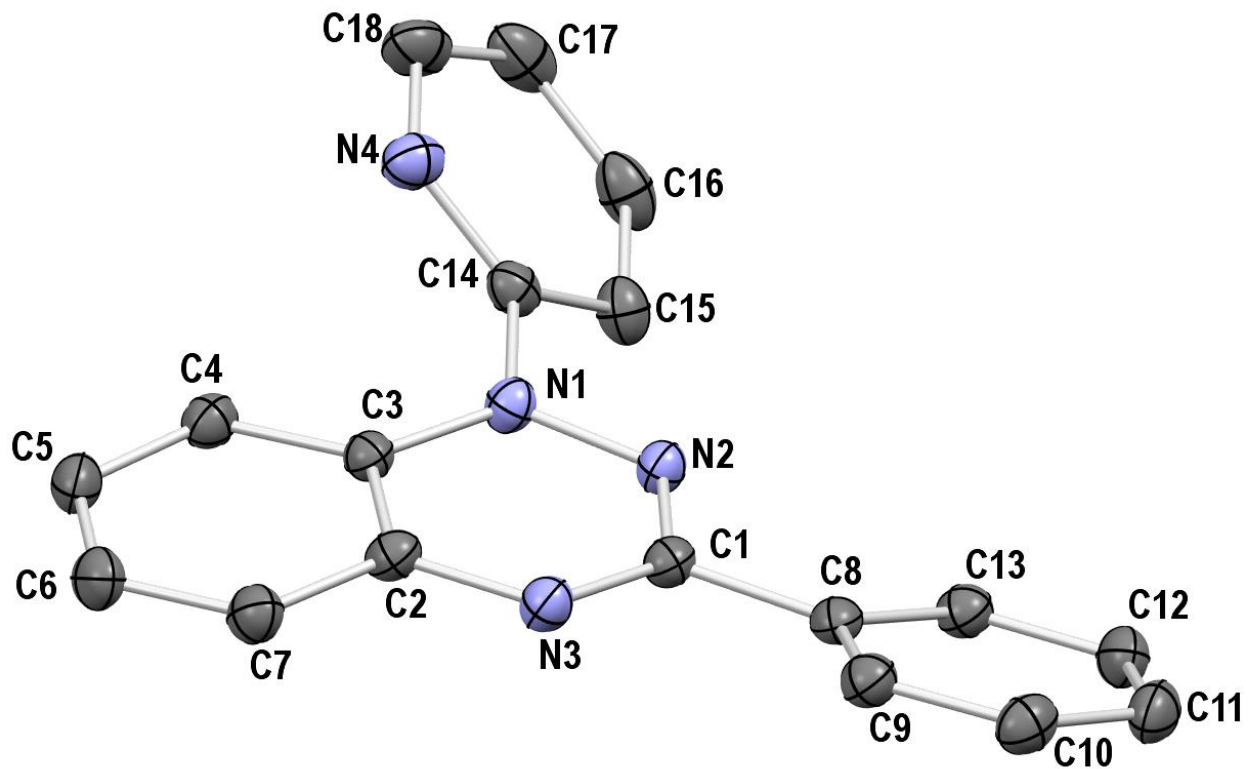
Fig. 2 ORTEP view of the 3-(phenyl)-1-(pyrid-2-yl)-1,4-dihydrobenzo[*e*][1,2,4]triazin-4-yl radical (50% probability of the thermal ellipsoids) in the crystal structure of (top) the polymorph **2α** and (bottom) the polymorph **2β**, along with the crystallographic atom numbering used in the discussion of X-ray structures. Hydrogens are omitted for clarity.

The 1,2,4-amidrazonyl moiety of polymorph **2β** is closer to planarity with deviation of the N1 and N3 atoms from the mean plane of C2, C3, N2, C1 of 0.06 and 0.03 Å, respectively (Fig. 2, bottom). The torsion angle (C3, N1, C14, N4) of the N1-(pyrid-2-yl) group with respect to the plane of benzotriazine is similar for both polymorphs [38.9(3) and 36.4(2)° for **2α** for **2β**, respectively] and significantly less than the average of 59±13° reported thus far.[19] This torsion angle is the result of steric repulsion between the H4 and the lone pair of N4. The torsion angle (N3, C1, C8, C9) between the C3-phenyl and the amidrazonyl plane is 15.3(3)° and 0.8(2)° for **2α** and **2β**, respectively. Despite subtle differences in the intramolecular geometrical parameters of the radicals in these two polymorphs, their solid-state packing presents some striking distinctions in the way these radicals associate and π stack.

Most benzotriazinyls form 1D supramolecular arrangements wherein the radicals π stack to obtain efficient SOMO-SOMO overlap.[21-33] This is also the case for both polymorphs **2α** and **2β**, and is attributed to the presence of the spin density primarily on the amidrazonyl unit (*ca*. 70%) and to a lesser degree on the fused benzene ring and the N1-(pyrid-2-yl) substituent (*vide infra*).

Solid-state packing of polymorph **2α**. Polymorph **2α** π stacks along the *a*-axis and forms supramolecular chains of evenly spaced radicals (Fig. 3, left). A 2-fold screw axis in the [1, 0, 0]

direction at *x*, 1/4, 0 and screw component [1/2, 0, 0] places the N1-(pyrid-2-yl) substituent directly on top of a triazine ring (eclipsed conformation) of a subsequent radical inside the π stack to form a "head-to-tails" dimer (Fig. 3, left). This packing is unique as most benzotriazinyls overlap in either a centrosymmetric manner or *via* translation parallel to the stacking direction. The centroid distance between these two N1-(pyrid-2-yl) and 1,2,4-triazine rings is 3.48 Å. There are three pairs of close intermolecular contacts between radicals inside the π stack, C16···C2 [d = 3.388(3) Å], C15···C4 [d = 3.390(3) Å] and C9···C17 [d = 3.323(4) Å]. These contacts are significantly shorter than the sum of the van der Waals radii, reflecting strong interactions between spin density sites. Neighbouring π stacks are related *via* two 2-fold axes. One along the *b*-axis at 0, *y*, 1/4 with screw component [0, 1/2, 0] and one along the *c*-axis at 1/4, 0, *z* with screw component [0, 0, 1/2]. These neighbouring stacks are connected *via* rich network of close intermolecular contacts and proximity interactions to form tight packing without significant voids. These include two weak hydrogen bonds C10-H10···N4 (d = 2.650 Å) [C10···N4, d = 3.571(3) Å, ∠C10-H10···N4 = 171.0°], C12-H12···N3 (d = 2.714 Å) [C12···N3, d = 3.556(3) Å, ∠C12-H12···N3 = 150.9°] and a short non-stabilizing interaction C7-H7···H16 [d = 2.367 Å, C7···C16, d = 3.914(3) Å, ∠C7-H7···H16 = 128.0°].
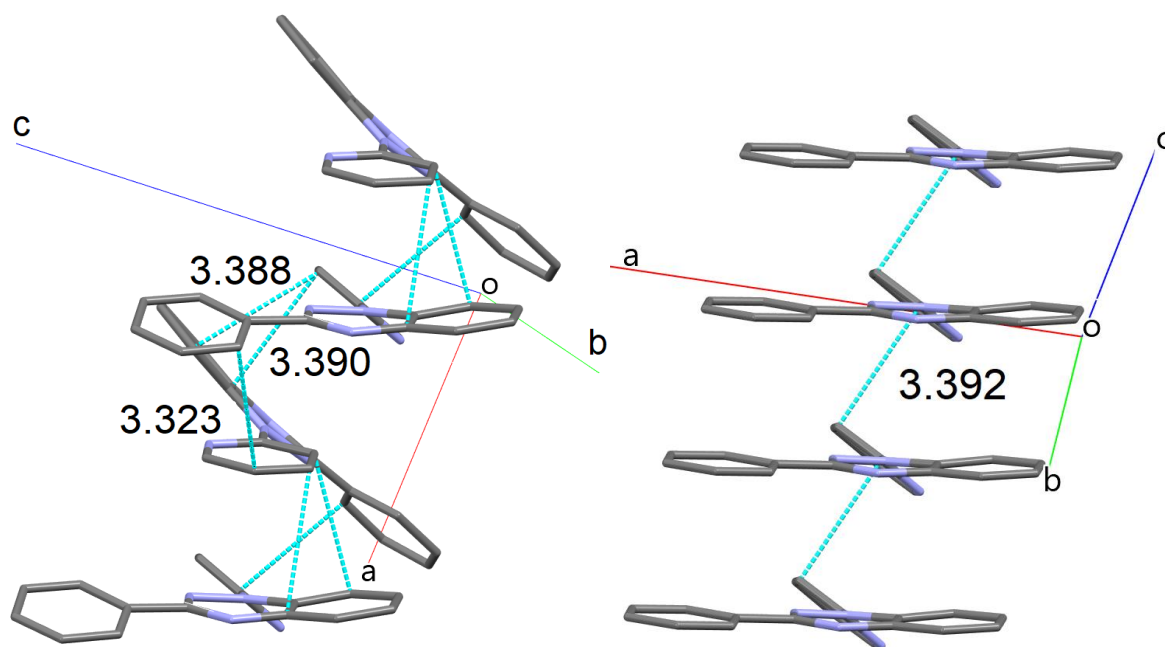
Fig. 3 Supramolecular chains of π stacked radicals in (left) polymorph **2α** along the crystallographic *a*-axis and (right) in polymorph **2β** along the crystallographic *b*-axis. Shortest intermolecular contacts inside the π stacks, measured in Å, shown in blue dotted lines. Hydrogen atoms are omitted for clarity.

Solid-state packing of polymorph **2β**. Radicals in polymorph **2β** π stack along the *b*-axis to form supramolecular chains of evenly spaced radicals (Fig. 3, right). The molecules inside the stack are related *via* a glide plane perpendicular to [0, 1, 0] with glide component [0, 0, 1/2] packing in a "head-to-head" orientation. This results in a slipped π stack wherein the radicals are not eclipsed but overlap with slippage angles of 76.45° (longitudinal) and 70.75° (latitudinal). The interplanar distance along the supramolecular chains (defined as the distance between subsequent planes of benzotriazinyl rings) is 3.432 Å (Fig. 3, right). The shortest contact inside the π stack is between carbons of the N1-(pyrid-2-yl) substituent C14···C15 [$d = 3.392(2)$ Å]. Neighbouring π stacks are connected *via* two weak hydrogen bonds, C5-H5···N4 ($d = 2.648$ Å) [C5···N4, $d = 3.540(2)$ Å,

∠C5-H5···N4 = 160.9°], C17-H17···N3 (d = 2.600 Å) [C17···N3, d = 3.507(2) Å, ∠C17-H17···N3 = 165.3°] and a non-stabilizing interaction C9-H9···C17 [d = 2.899 Å, C9···C17, d = 3.734(2) Å, ∠C9-H9···C17 = 150.4°] in "head-to-tail" orientation to form chains along the c-axis (Fig. 4). Neighbouring chains are related by an inversion centre at [0, 0, 0] and a 2-fold screw axis with direction [0, 1, 0] at 0, y, 1/4 and screw component [0, 1/2, 0]. These antiparallel chains run along the a-axis (Figure 4) and are connected by short C5-H5···N4 contacts (d = 2.648 Å) [C5···N4, d = 3.540(2) Å, ∠C5-H5···N4 = 160.9°].
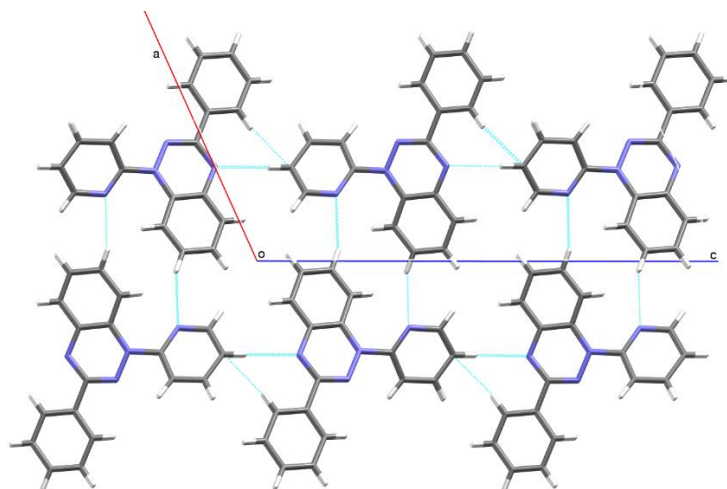

Fig. 4 View of crystal packing of polymorph **2β** perpendicular to the crystallographic ac-plane showing intermolecular contacts between neighbouring π stacks.

Before measuring the magnetic properties of polymorphs **2α** and **2β**, analytical data were collected to confirm their chemical purity and as well as their powder X-ray diffraction patterns (Fig. 5).
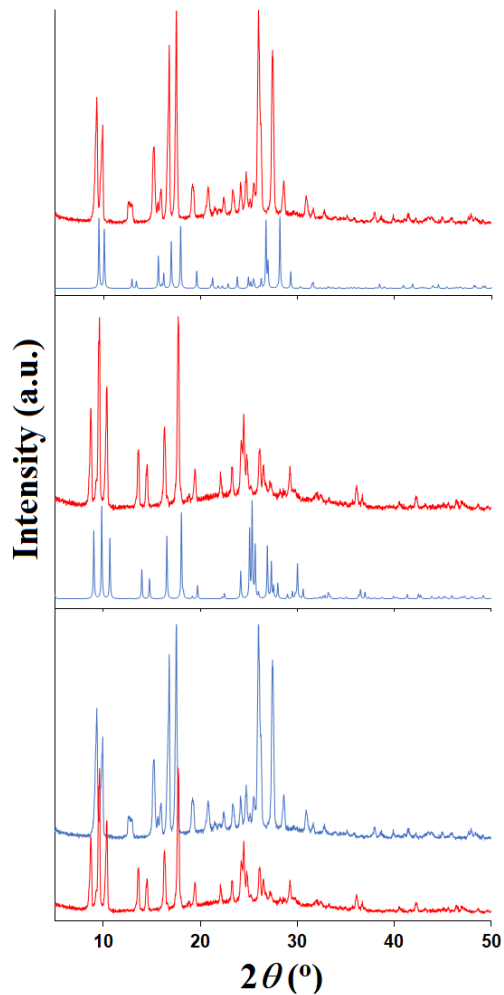
Fig. 5 Powder X-ray diffraction patterns of samples used for magnetic measurements: (top) **2α** collected at 300 K (red line) and calculated from the single crystal X-ray structure at 100 K (blue line), (middle) **2β** collected at 300 K (red line) and calculated from the single crystal X-ray structure at 100 K (blue line) and (bottom) comparison of the experimental powder X-ray diffraction patterns at 300 K for the two polymorphs **2α** (blue line) and **2β** (red line).

The experimental diffraction signatures of polycrystalline samples at 300 K for **2α** and **2β** match well the patterns calculated from single crystal X-ray structures at 100 K. Additionally, the comparison of powder X-ray diffraction patterns for polymorphs demonstrates their phase purity.

However, the presence of small amounts of amorphous paramagnetic impurities cannot be fully excluded.

3.2 Magnetic Properties

The temperature dependence of the magnetic susceptibility (χ) was collected on polycrystalline samples of **2α** and **2β** in the 2-300 K temperature region. The representative data are shown as χ vs. T and χT vs. T plots in Figure 6. The χT product at 300 K is 0.34 and 0.29 cm^3 K mol^{-1} for **2α** and **2β**, respectively. These values are significantly smaller than the expected Curie constant of 0.375 cm^3 mol^{-1} K expected for an $S = \frac{1}{2}$ radical species with a g factor of 2. This apparent discrepancy is induced by the presence of significant antiferromagnetic interactions between radical molecules as confirmed by the marked decrease of the χT product (or the broad maximum of the magnetic susceptibility at 47 and 100 K, respectively) when decreasing the temperature. At 2 K, if one considers that the χT product should be null when all the radical spins are fully antiferromagnetically coupled, the observed residual paramagnetism of 0.004 and 0.006 cm^3 K mol^{-1}, respectively, corresponds to about 1 and 2 % of an $S = \frac{1}{2}$ Curie impurity. Based on the crystal structures shown above, the strongest antiferromagnetic interactions should be present along the regular chain of radicals in both polymorphs (Figure 3). The magnetic susceptibility data were thus modeled using a regular chain of $S = \frac{1}{2}$ quantum spins with a single magnetic interaction, J, between radical centers ($\boldsymbol{H} = -2J\ \Sigma S_i S_{i+1}$). The analytical expression of the susceptibility established by Bonner and Fischer in 1964,[91-93] was used to fit both χ vs. T and χT vs. T plots shown in Figure 6 (solid red line). For both polymorphs, the regular chain model is able to reproduce well the experimental data with an estimated intrachain exchange coupling, J/k_B = − 36.7(3) K (−25.5(2) cm^{-1}; between 300 and 15 K) for **2α** and J/k_B = −72(3) K (−50(2) cm^{-1};

between 300 and 20 K) for **2β** (with *g* factor of 2.05(5) for both compounds). It should be mentioned that the magnetic properties for **2α** and **2β** have been measured on different samples (three and four, respectively; See Figure S2) with a good reproducibility of data shown in Figure 6 (the above *J* values are those of sample 1 in Figure S2; the values for the other samples are given in the Figure S2 caption).

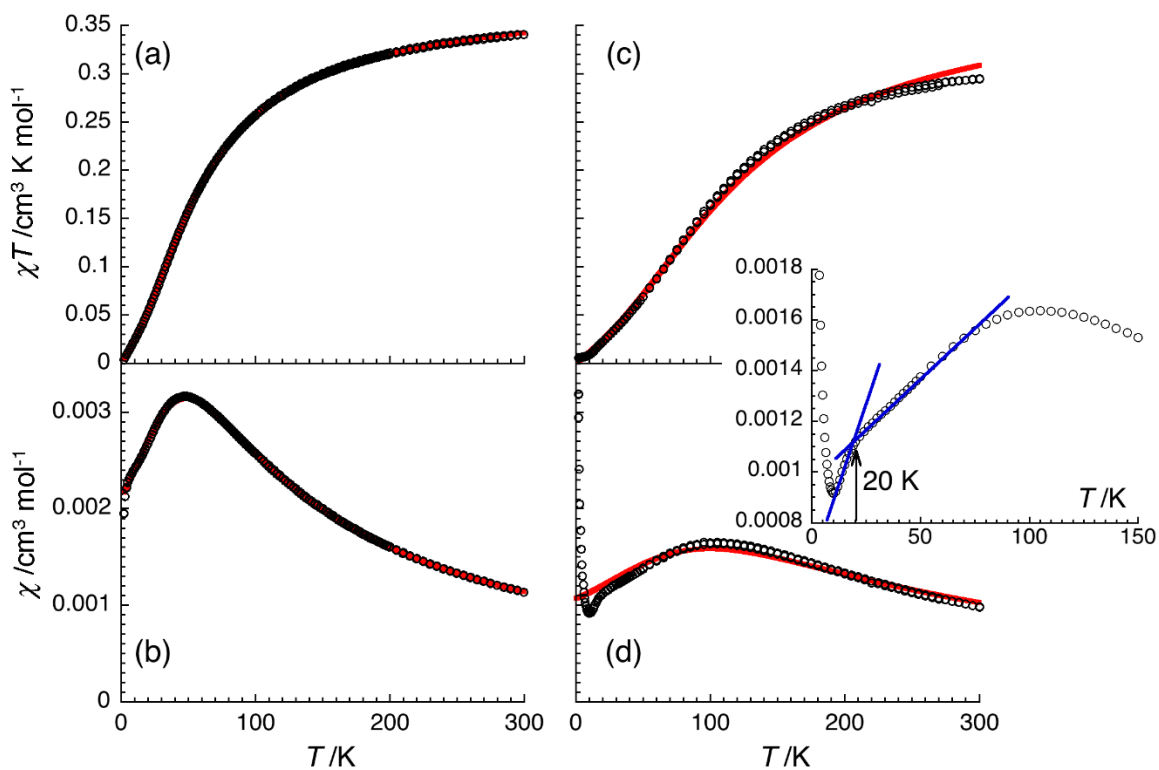**Fig. 6** Temperature dependence of (bottom) the magnetic susceptibility and (top) the χT product for polymorphs (left; at 0.5 T) **2α** and (right; at 0.1 T) **2β** (χ is defined as *M/H* per mole of radical **2**). The solid red lines are the best fit of the experimental data to the regular chain model of antiferromagnetically coupled quantum spins developed by Bonner and Fisher;[91-93] see text for details.

While the regular chain model is perfect for the magnetic data of **2α**, the theory/experiment agreement for **2β** is obviously less performant. Hence, alternative spin chain models with two different magnetic interactions have also been considered without being able to significantly improve the agreement. It is thus suspected that interchain magnetic interactions are indeed effective in polymorph **2β**. Below 20 K (Figure 6, inset), a clear anomaly is observed on the susceptibility of polymorph **2β**, indicating a possible phase transition. Attempts to collect the crystal structure of polymorph **2β** at 3 K led to diffraction degradation in one direction which appeared to be reversible. The magnetic and X-ray diffraction experimental data suggested a phase transition below 17 K that most likely involves a dimerization of the radicals along the chain as observed in many related 1D spin systems.[94-99]

3.3 DFT and ab-initio calculations

Magnetism-structure correlations can be further supported by means of quantum chemical methods.[100] This is typically done either at post-HF levels or using BS-DFT of which the latter is a computationally efficient but theoretically less-rigorous approach that is typically employed for systems containing several tens, even hundreds, of atoms.

Table 1 Exchange-coupling constants J_{comp} (cm^{-1}) calculated for polymorphs **2α** and **2β** with BS-DFT and def2-TZVPP basis sets.

	B3LYP	X3LYP	CAM-B3LYP	ωB97x	LC-ωHPBE	M062X	MN15
2α	−30.5	−28.9	−15.2	−11.4	−8.9	−23.3	−25.0
2β	−29.5	−27.1	−5.5	4.1	10.3	−6.8	−31.7

Table 1 lists the exchange-coupling constants calculated for polymorphs 2α and 2β using different density functionals. The data can be compared to the experimentally determined radical···radical interactions, -25.5 and -50 cm^{-1} for polymorph 2α and 2β, respectively. In general, all functionals predict the coupling in 2α to be antiferromagnetic but the coupling strength varies greatly between different functionals. Most notably, functionals with improved long-range corrections, namely CAM-B3LYP, ωB97x and LC-ωHPBE, predict significantly weaker antiferromagnetic coupling compared to others, which, surprisingly, show only small variation and are in good agreement with the experimentally derived exchange coupling. The results for 2β are, however, more varied with some of the theoretically more just long-range corrected functionals even predicting the coupling to be ferromagnetic and, thus, at variance with experimental observations. It is also notable that even the best-performing functionals give J_{comp} for 2β that is almost half (in magnitude) of the experimentally derived intrachain exchange coupling J. The reason for this discrepancy is unclear, though it can be related to problems in treating the singlet state *via* BS-DFT and it also parallels the problems observed in modelling the magnetic data of 2β with the regular chain model. It should also be noted that by simple examination of the SOMO and the associated spin density of radical **2** (Fig. 7), it is evident that the benzo triazinyl ring contains most of the spin density and overlap through this region, like that in polymorph 2β., should lead to strong antiferromagnetic exchange interaction unless prevented by appropriate stack slippage. However, if the radicals pack so that the interactions involve the N1-(pyrid-2-yl) substituents, such as in polymorph 2α, the antiferromagnetic interaction is expected to be weaker even in case of perfect stacking due to less efficient overlap.
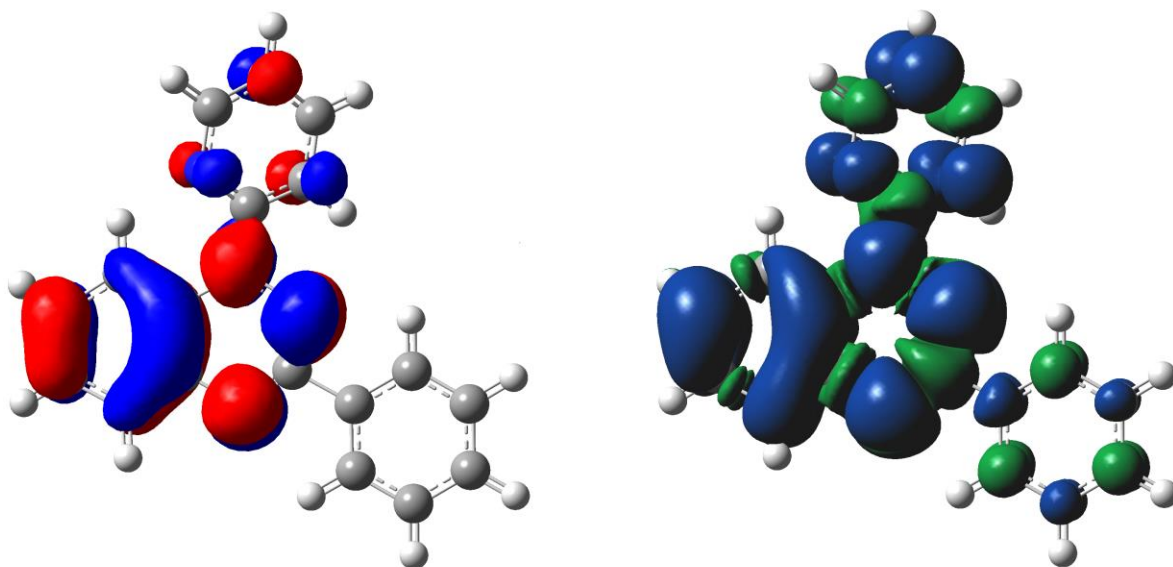
Fig. 7. Figures of the (left) SOMO and (right) spin density of radical **2** at the B3LYP/def2-TZVPP level of theory using isodensity values ±0.03 and ±0.0004, respectively

4. Conclusions

3-(Phenyl)-1-(pyrid-2-yl)-1,4-dihydrobenzo[*e*][1,2,4]triazin-4-yl (**2**) is the first example of a polymorphic Blatter-type radical. Two polymorphs, **2α** and **2β**, were identified, isolated and characterized by means of single crystal X-ray diffractometry and magnetic susceptibility measurements. Polymorph **2α** shows a unique mode of overlap along the 1D stacking direction where the N1-(pyrid-2-yl) substituent interacts face-to-face (eclipsed conformation) with a 1,2,4-triazinyl ring of a subsequent radical. Polymorph **2β** forms a slipped 1D π stack wherein the radicals overlap extensively over the benzotriazinyl rings.

Magnetic susceptibility studies reveal that in both cases the radical···radical interactions are antiferromagnetic. The intra-chain magnetic exchange interaction of polymorph **2β** (–50 cm^{-1}) was found to be double that of polymorph **2α** (–25.5 cm^{-1}), possibly due to more effective SOMO-SOMO overlap. The two low dimensional polymorphs of radical **2** demonstrate weak

antiferromagnetic interactions often observed in organic open-shell molecules.[101-102] While recent advances in the chemistry of organic radicals led to some materials exhibiting substantial magnetic hysteresis (primarily in thiazyl radicals),[103-107] this class of Blatter radicals have yet to demonstrate their efficiency to generate large magnetic couplings and thus magnetic order at high temperature as observed often in purely inorganic systems and in a few metal-organic materials.[108] Polymorphism in Blatter-type radicals could be more prevalent than heretofore recognized and requires careful examination of the harvested crystals. We are currently working on other examples of a Blatter-type radicals that demonstrate polymorphism.

Conflicts of interest

The authors declare no conflicts of interest.

Acknowledgements

References

1. H. M. Blatter and H. Lukaszewski, *Tetrahedron Lett.*, 1968, **9**, 2701-2705.

2. F. A. Neugebauer and I. Umminger, *Chem. Ber.*, 1980, **113**, 1205-1225.

3. F. A. Neugebauer and I. Umminger, *Chem. Ber.*, 1981, **114**, 2423-2430.

4. F. A. Neugebauer and G. Rimmler, *Magn. Reson. Chem.*, 1988, **26**, 595-600.

5. M. K. Kadirov, A. V. Il'yasov, A. A. Vafina, B. I. Buzykin, N. G. Gazetdinova and Y. P. Kitaev, *Bull. Acad. Sci. USSR, Div. Chem. Sci.*, 1984, **33**, 649-650.

6. K. Mukai, K. Inoue, N. Achiwa, J. B. Jamali, C. Krieger and F. A. Neugebauer, *Chem. Phys. Lett.*, 1994, **224**, 569-575.

7. K. A. Hutchison, G. Srdanov, R. Menon, J.-C. P. Gabriel, B. Knight and F. Wudl. *J. Am. Chem. Soc.*, 1996, **118**, 13081-13082.

8. C. P. Constantinides and P. A. Koutentis, *Adv. Heterocycl. Chem.*, 2016, **119**, 173-207.

9. N. M. Gallagher, J. J. Bauer, M. Pink, S. Rajca and A. Rajca, *J. Am. Chem. Soc.*, 2016, **138**, 9377-9380.

10. C. P. Constantinides, P. A. Koutentis, H. Krassos, J. M. Rawson and A. J. Tasiopoulos, *J. Org. Chem.*, 2011, **76**, 2798-2806.

11. P. A. Koutentis and D. Lo Re, *Synthesis*, 2010, **2010**, 2075-2079.

12. A. A. Berezin, C. P. Constantinides, S. I. Mirallai, M. Manoli, L. L. Cao, J. M. Rawson and P. A. Koutentis, *Org. Biomol. Chem.*, 2013, **11**, 6780-6795.

13. A. A. Berezin, G. Zissimou, C. P. Constantinides, Y. Beldjoudi, J. M. Rawson and P. A. Koutentis, *J. Org. Chem.*, 2014, **79**, 314-327.

14. A. C. Savva, S. I. Mirallai, G. A. Zissimou, A. A. Berezin, M. Demetriades, A. Kourtellaris, C. P. Constantinides, C. Nicolaides, T. Trypiniotis and P. A. Koutentis, *J. Org. Chem.*, 2017, **82**, 7564-7575.

15. A. A. Berezin, C. P. Constantinides, C. Drouza, M. Manoli and P. A. Koutentis, *Org. Lett.*, 2012, **14**, 5586-5589.

16. C. P. Constantinides, P. A. Koutentis and G. Loizou, *Org. Biomol. Chem.*, 2011, **9**, 3122-3125.

17. C. P. Constantinides, E. Obijalska and P. Kaszynski, *Org. Lett.*, 2016, **18**, 916-919.

18. J. A. Grant, Z. Lu, D. E. Tucker, B. M. Hockin, D. S. Yufit, M. A. Fox, R. Kataky, V. Chechik and A. M. C. O'Donoghue, *Nat. Commun.*, 2017, **8**, 15088.

19. P. Kaszynski, C. P. Constantinides and V. G. Young, *Angew. Chem. Int. Ed.*, 2016, **55**, 11149-11152.

20. Y. Takahashi, Y. Miura and N. Yoshioka, *Chem. Lett.*, 2014, **43**, 1236-1238.

21. C. P. Constantinides, P. A. Koutentis and J. M. Rawson, *Chem. - Eur. J.*, 2012, **18**, 15433-15438.

22. C. P. Constantinides, A. A. Berezin, M. Manoli, G. M. Leitus, G. A. Zissimou, M. Bendikov, J. M. Rawson and P. A. Koutentis, *Chem. - Eur. J.*, 2014, **20**, 5388-5396.

23. C. P. Constantinides, P. A. Koutentis and J. M. Rawson, *Chem. - Eur. J.*, 2012, **18**, 7109-7116.

24. C. P. Constantinides, A. A. Berezin, M. Manoli, G. M. Leitus, M. Bendikov, J. M. Rawson and P. A. Koutentis, *New J. Chem.*, 2014, **38**, 949-954.

25. C. P. Constantinides, A. A. Berezin, G. A. Zissimou, M. Manoli, G. M. Leitus, M. Bendikov, M. R. Probert, J. M. Rawson and P. A. Koutentis, *J. Am. Chem. Soc.*, 2014, **136**, 11906-11909.

26. C. P. Constantinides, E. Carter, D. M. Murphy, M. Manoli, G. M. Leitus, M. Bendikov, J. M. Rawson and P. A. Koutentis, *Chem. Commun.*, 2013, **49**, 8662-8664.

27. C. P. Constantinides, A. A. Berezin, G. A. Zissimou, M. Manoli, G. M. Leitus and P. A. Koutentis, *Molecules*, 2016, **21**, 636 (1-7).

28. Y. Takahashi, R. Matsuhashi, Y. Miura and N. Yoshioka, *Chem. - Eur. J.*, 2018, **24**, 7939-7948.

29. Y. Takahashi, N. Tsuchiya, Y. Miura and N. Yoshioka, *New. J. Chem.*, 2018, **42**, 9949-9955.

30. Y. Zheng, M.-s. Miao, M. C. Kemei, R. Seshadri and F. Wudl, *Isr. J. Chem.*, 2014, **54**, 774-778.

31. Y. Miura and N. Yoshioka, *Chem. Phys. Lett.*, 2015, **626**, 11-14.

32. X. Hu, L. Zhao, H. Chen., Y. Ding, Y.-Z. Zheng, M.-s. Miao and Y. Zheng, *J. Mater. Chem. C*, 2019, **7**, 6559-6563.

33. B. Yan, J. Cramer, R. McDonald and N. L. Frank, *Chem. Commun.*, 2011, **47**, 3201-3203.

34. Y. Takahashi, Y. Miura and M. Yoshioka, *New J. Chem.*, 2015, **39**, 4783-4789.

35. M. Demetriou, A. A. Berezin, P. A. Koutentis and T. Krasia-Christoforou, *Polym. Int.*, 2014, **63**, 674-679.

36. J. Areephong, K. M. Mattson, N. J. Treat, S. O. Poelma, J. W. Kramer, H. A. Sprafke, A. A. Latimer, J. Read de Alaniz and C. J. Hawker, *Polym. Chem.*, 2016, **7**, 370-374.

37. J. Areephong, N. Treat, J. W. Kramer, M. D. Christianson, C. J. Hawker and H. A. Collins, *WO Pat.*, 061189A1, 2015.

38. F. J. M. Rogers and M. L. Coote, *J. Phys. Chem. C*, 2019, **123**, 10306-10310.

39. I. S. Morgan, A. Peuronen, M. M. Hänninen, R. W. Reed, R. Clérac and H. M. Tuononen, *Inorg. Chem.*, 2014, **53**, 33-35.

40. I. S. Morgan, A. Mansikkamäki, G. A. Loizou, P. A. Koutentis, M. Rouzières, R. Clérac and H. M. Tuononen, *Chem. - Eur. J.*, 2015, **21**, 15843-15853.

41. I. S. Morgan, A. Mansikkamäki, M. Rouzières, R. Clérac and H. M. Tuononen, *Dalton Trans.*, 2017, **46**, 12790-12793.

42. N. M. Gallagher, J. J. Bauer, M. Pink, S. Rajca and A. Rajca, *J. Am. Chem. Soc.*, 2016, **138**, 9377-9380.

43. N. Gallagher, H. Zhang, T. Junghoefer, E. Giangrisostomi, R. Ovsyannikov, M. Pink, S. Rajca, M. B. Casu and A. Rajca, *J. Am. Chem. Soc.*, 2019, **141**, 4764-4774.

44. F. Ciccullo, N. M. Gallagher, O. Geladari, T. Chassé, A. Rajca and M. B. Casu, *ACS Appl. Mater. Interfaces*, 2016, **8**, 1805-1812.

45. M. B. Casu, *Acc. Chem. Res.*, 2018, **51**, 753-760.

46. J. Z. Low, G. Kladnik, L. L. Patera, S. Sokolov, G. Lovat, E. Kumarasamy, J. Repp, L. M. Campos, D. Cvetko, A. Morgante and L. Venkataraman, *Nano Lett.*, 2019, **19**, 2543-2548.

47. L. L. Patera, S. Sokolov, J. Low, L. Campos, L. Venkataraman and J. Repp, *Angew. Chem. Int. Ed.*, 2019, **131**, 11179-11183.

48. F. Ciccullo, A. Calzolari, K. Bader, P. Neugebauer, N. M. Gallagher, A. Rajca, J. van Slageren and M. B. Casu, *ACS Appl. Mater. Interfaces*, 2019, **11**, 1571-1578.

49. Y. Zhang, Y. Zheng, H. Zhou, M.-S. Miao, F. Wudl and T.-Q. Nguyen, *Adv. Mater.*, 2015, **27**, 7412-7419.

50. Y. Zheng, M.-S. Miao, G. Dantelle, N. D. Eisenmenger, G. Wu, I. Yavuz., M. L. Chabinyc, K. N. Houk and F. Wudl, *Adv. Mater.*, 2015, **27**, 1718-1723.

51. G. Karecla, P. Papagiorgis, N. Panagi, G. A. Zissimou, C. P. Constantinides, P. A. Koutentis, G. Itskos and S. C. Hayes, *New J. Chem.*, 2017, **41**, 8604-8613.

52. M. Jasinski, S. Kapuscinski and P. Kaszynski, *J. Mol. Liq.*, 2019, **277**, 1054-1059.

53. M. Jasinski, K. Szymanska, A. Gardias, D. Pociecha, H. Monobe, J. Szczytko and P. Kaszynski, *ChemPhysChem*, 2019, **20**, 636-644.

54. S. Kapuscinski, A. Gardias, D. Pochiecha, M. Jasinski, J. Szczytko and P. Kaszynksi, *J. Mater. Chem. C*, 2018, **6**, 3079-3088.

55. M. Jasinski, J. Szczytko, D. Pochiecha, H. Monobe and P. Kaszynski, *J. Am. Chem. Soc.*, 2016, **138**, 9421-9424.

56. B. Häupler, U. S. Schubert, A. Wild, P. A. Koutentis and G. Zissimou, *DE Pat.*, 102017005 924A1, 2018.

57. J. S. Miller, *Adv. Mater.*, 1998, **10**, 1553-1557.

58. J. Haleblian and W. McCrone, *J. Pharm. Sci.*, 1969, **58**, 911-929.

59. Y. Beldjoudi, A. Arauzo, F. Palacio, M. Pilkington and J. M. Rawson, *J. Am. Chem. Soc.* 2016, **138**, 16779-16786.

60. Y. Beldjoudi, A. Arauzon, J. Campo, E. L. Gavey, M. Pilkington, M. A. Nascimento and J. M. Rawson, *J. Am. Chem. Soc.*, 2019, **141**, 6875-6889.

61. A. Alberola, O. P. Clements, R. J. Collis, L. Cubbitt, C. M. Grant, R. J. Less, R. T. Oakley, J. M. Rawson, R. W. Reed and C. M. Robertson, *Cryst. Growth Des.*, 2008, **8**, 155-161.

62. A. Alberola, C. S. Clarke, D. A. Haynes, S. I. Pascu and J. M. Rawson, *Chem. Commun.* 2005, 4726-4728.

63. C. S. Clarke, D. A. Haynes, J. N. M. Smith, A. S. Batsanov, J. A. K. Howard, S. I. Pascu and J. M. Rawson, *CrystEngComm*, 2010, **12**, 172-185.

64. E. M. Fatila, M. C. Jennings, J. Goodreid and K. E. Preuss, *Acta Crystallogr., Sect C: Cryst. Struct. Commun.*, 2010, **66**, o260-o264.

65. A. D. Bond, D. A. Haynes, C. M. Pask and J. M. Rawson, *J. Chem. Soc., Dalton Trans.* 2002, 2522-2531.

66. C. S. Clarke, S. I. Pascu and J. M. Rawson, *CrystEngComm*, 2004, **6**, 79-82.

67. C. Knapp, E. Lork, K. Gupta and R. Z. Mews, *Z. Anorg. Allg. Chem.*, 2005, **631**, 1640-1644.

68. V. Kumar, S. Shova, V. Maurel, G. Novitchi and C. Train, *Eur. J. Inorg. Chem.*, 2018, 517-524.

69. R. C. Clark and J. S. Reid, *Acta Cryst.*, 1995, **A51**, 887-897.

70. G. M. Sheldrick, *Acta Cryst. A*, 2008, **64**, 112-122.

71. G. M. Sheldrick, *Acta Cryst. C*, 2015, **71**, 3-8.

72. C. F. Macrae, P. R. Edgington, P. McCabe, E. Pidcock, G. P. Shields, R. Taylor, M. Towler and J. van de Streek, *J. Appl. Cryst.*, 2006, **39**, 453-457.

73. G. A. Bain and J. F. Berry, *J. Chem. Educ.*, 2008, **85**, 532-536.

74. L. Noodleman, *J. Chem. Phys.*, 1981, **74**, 5737-5743.

75. F. Weigend, R. Ahrlichs. *Phys. Chem. Chem. Phys.* **2005**, *7*, 3297-3305.

76. Becke, A. D. *Phys. Rev. A* 1988, **38**, 3098.

77. C. Lee, W. Yang and R. G. Parr, *Phys. Rev. B*, 1998, **37**, 785-789.

78. X. Xu, Q. Zhang, R. P. Muller and W. A. Goddard, *J. Chem. Phys.*, 2005, **122**, 14105.

79. T. Yanaia, D. P. Tewb, N. C. Handy *Chem. Phys. Lett.* 2004, **393**, 51-57.

80. J.-D. Chai and M. Head-Gordon, *J. Chem. Phys.,* 2008, **128**, 84106.

81. T. M. Henderson, A. F. Izmaylov, G. Scalmani, and G. E. Scuseria, *J. Chem. Phys.*, 2009 **131,** 044108.

82. O.A. Vydrov and G. E. Scuseria, *J. Chem. Phys.*, 2006, **125**, 234109.

83. O. A. Vydrov, J. Heyd, A. Krukau, and G. E. Scuseria, *J. Chem. Phys.*, 2006, **125**, 74106.

84. O. A. Vydrov, G. E. Scuseria, and J. P. Perdew, *J. Chem. Phys.*, 2007, **126,** 154109.

85. Y. Zhao and D. G. Truhlar, *J. Chem. Phys.*, 2006, **125**, 194101.

86. Y. Zhao and D. G. Truhlar, *Theor. Chem. Acc.*, 2006, **120**, 215-241.

87. H. S. Yu, X. He, S. L. Li and D. G. Truhlar, *Chem. Sci.*, 2016*,* **7**, 5032-5051.

88. H. S. Yu, X. He, S. L. Li and D. G. Truhlar, *J. Chem. Theory Comput.*, 2016*,* **12**, 1280-1293.

89. M. J. Frisch, G. W. Trucks, H. B. Schlegel, G. E. Scuseria, M. A. Robb, J. R. Cheeseman, G. Scalmani, V. Barone, G. A. Petersson, H. Nakatsuji, X. Li, M. Caricato, A. V. Marenich, J. Bloino, B. G. Janesko, R. Gomperts, B. Mennucci, H. P. Hratchian, J. V. Ortiz, A. F. Izmaylov, J. L. Sonnenberg, D. Williams-Young, F. Ding, F. Lipparini, F. Egidi, J. Goings, B. Peng, A. Petrone, T. Henderson, D. Ranasinghe, V. G. Zakrzewski, J. Gao, N. Rega, G. Zheng, W. Liang, M. Hada, M. Ehara, K. Toyota, R. Fukuda, J. Hasegawa, M. Ishida, T. Nakajima, Y. Honda, O. Kitao, H. Nakai, T. Vreven, K. Throssell, J. A. Montgomery, Jr., J. E. Peralta, F. Ogliaro, M. J. Bearpark, J. J. Heyd, E. N. Brothers, K. N. Kudin, V. N. Staroverov, T. A. Keith, R. Kobayashi, J. Normand, K. Raghavachari, A. P. Rendell, J. C. Burant, S. S. Iyengar, J. Tomasi, M. Cossi, J. M. Millam, M. Klene, C. Adamo, R. Cammi,

J. W. Ochterski, R. L. Martin, K. Morokuma, O. Farkas, J. B. Foresman and D. J. Fox, *Gaussian 16, Revision B.01*, Gaussian, Inc., Wallingford CT, 2016.

90. J. Towns, T. Cockerill, M. Dahan, I. Foster, K. Gaither, A. Grimshaw, V. Hazlewood, S. Lathrop, D. Lifka, G. D. Peterson, R. Roskies, J. R. Scott and N. Wilkins-Diehr, *Comput. Sci. Eng.*, 2014, **16**, 62-74.

91. J. C. Bonner and M. E. Fisher, *Phys. Rev.*, 1964, **135**, A640-A658.

92. J. B. Torrance, Y. Tomkiewicz and B. D. Silverman, *Phys. Rev. B*, 1977, **15**, 4738-4749.

93. W. E. Estes, D. P. Gavel, W. E. Hatfield and D. J. Hodgson, *Inorg. Chem.*, 1978, **17**, 1415-1421.

94. J. W. Bray, L. V. Interrante, I. S. Jacobs and J. C. Bonner, *The Spin-Peierls Transition*, *In Extended Linear Chain Compound.*, J. S. Miller (Ed.), Springer, Boston, MA, 1983.

95. J.-P. Pouget, P. Alemany and E. Canadell, *Mater. Horiz.*, 2018, **5**, 590-640.

96. R. T. Clay and S. Mazumdar, *Phys. Rep*, 2019, **788**, 1-89.

97. A. Vasiliev, O. Volkova, E. Zvereva and M. Markina, *npj Quantum Mater.*, 2018, **3**, 18.

98. H.-B. Duan, X.-M. Ren and Q.-J. Meng, *Coord. Chem. Rev.*, 2010, **254**, 1509-1522.

99. C. Coulon and R. Clérac, *Chem. Rev.*, 2004, **104**, 5655-5687.

100. J. J. Novoa, M. Deumal and J. Jornet-Somoza, *Chem. Soc. Rev.*, 2011, **40**, 3182-3212.

101. R. G. Hicks, *Stable radicals: Fundamentals and Applied Aspects of Odd-Electron Compounds*, Wiley, 2010.

102. I. Ratera and J. Veciana, *Chem. Soc. Rev.*, 2012, **41**, 303.

103. J. M. Rawson and J. J. Hayward, *Spin Crossover Materials: Properties and Applications*, M. A. Halcrow (Ed.), Wiley: Chichester, U. K., 2013, Chapter 8.

104. W. Fujita and K. Awaga, *Science*, 1999, **286**, 261-262.

105. G. D. McManus, J. M. Rawson, N. Feeder, E. J. L. McInnes, J. J. Novoa, R. Burriel, F. Palacio and P. Oliete, *J. Mater. Chem.*, 2001, **11**, 1992-2003.

106. J. L. Brusso, O. P. Clements, R. C. Haddon, M. E. Itkis, A. A. Leitch, R. T. Oakley, R. W. Reed and J. F. Richardson, *J. Am. Chem. Soc.*, 2004, **126**, 14692-14693.

107. A. Alberola, J. Burley, R. J. Collis, R. J. Less and J. M. Rawson, *J. Organomet. Chem.*, 2007, **692**, 2750-2760.

108. J. M. Rawson and C. P. Constantinides, *Thiazyl Magnets,* World Scientific Reference On Spin in Organics, J. S. Miller (Ed.), 2018, **4**, 95-124.